

Study and mathematical analysis of the novel fractional bone mineralization model

RITU AGARWAL^{1*}, CHHAYA MIDHA²

^{1,2}Department of Mathematics, Malaviya National Institute of Technology, Jaipur-302017, INDIA

E-mail: ¹*ragarwal.maths@mnit.ac.in*, ²*midhachhaya@gmail.com*

Abstract

Different biological models can be evaluated using mathematical models in both qualitative and quantitative ways. A fractional bone mineralization model involving Caputo's fractional derivative is presented in this work. The fractional mathematical model is beneficial because of its memory carrying property. An appropriate fractional order of the derivative can be chosen that is more closely related to experimental or actual data. The dynamical system of equations for the process of bone mineralization is examined qualitatively and quantitatively in this article. A numerical simulation has been performed for the model. The model's parameters have undergone sensitivity analysis and their effects on the model variables have been explored. By studying the mineralization patterns in bone, different diseases can be cured, and it can also be examined how the deviations from healthy mineral distributions lead to specific bone diseases.

Keywords Bone mineralization, mineralization dynamics, Caputo fractional derivative, critical points

2020 Mathematics subject classification:92-10, 34A34

1 Introduction

In the last decades fractional calculus had a remarkable journey in the field of science, mathematics, and physics. Numerous fractional calculus applications include biophysics, polymer material research, heat transmission in biological systems, random walk problems, and chaotic systems description. (see, e.g [7, 8, 13, 21]). Dynamics of some other models have also been studied like the Ebola virus model [15], malaria transmission model [20], and tumour growth model[9, 19]. Some other biological models and their mathematical analysis can be found in [16, 17, 18].

*Corresponding Author

The Riemann-Liouville fractional integral of order ϱ , $0 < \varrho \leq 1$ of the function $f \in L_1[a, b]$ is defined as

$$I_x^\varrho f(x) = \frac{1}{\Gamma(\varrho)} \int_0^x (x-t)^{\varrho-1} f(t) dt. \tag{1}$$

Caputo fractional derivative, named after Michele Caputo, was first mentioned in his research article [5] in 1967.

Definition 1.1 (Caputo Fractional Derivative). *Suppose that $\varrho > 0$, $a < x < b$, $x \in \mathbb{R}$ and $f(x) \in AC^n[a, b]$, the fractional operator*

$${}_a^C D_x^\varrho f(x) = \frac{1}{\Gamma(n-\varrho)} \int_a^x (x-t)^{n-\varrho-1} f^{(n)}(t) dt, \quad n = [Re(\varrho)] + 1, \tag{2}$$

is called the Caputo fractional derivative of order ϱ .

Equivalently, in the convolution form

$${}_a^C D_x^\varrho f(x) = \frac{1}{\Gamma(n-\varrho)} f^{(n)}(x) * (x^{n-\varrho-1}), \quad n = [Re(\varrho)] + 1, \quad x \in (a, b). \tag{3}$$

The Caputo derivative of the power function x^n is given by

$${}_0^C D_x^\varrho (x^n) = \frac{\Gamma(1+n)}{\Gamma(n+1-\varrho)} x^{n-\varrho}. \tag{4}$$

The composition of the Caputo fractional derivative and Riemann-Liouville fractional integral gives the following results:

$$\begin{aligned} ({}_0^C D_x^\varrho I_x^\varrho f)(x) &= f(x), \tag{5} \\ (I_x^\varrho {}_0^C D_x^\varrho f)(x) &= f(x) - \sum_{k=0}^{n-1} f^{(k)}(0^+) \frac{(x-\varrho)^k}{k!}. \tag{6} \end{aligned}$$

We aim to study the dynamics of bone mineralization by fractionalising it in the Caputo sense, followed by finding its solution and graphical analysis.

2 Bone mineralization

Bone is a multidimensional system that functions as a mechanical shield to provide support and security. The involvement of bone in haemostasis (cessation of bleeding from a blood vessel) is also crucial. The process of developing inorganic precipitation over an organic foundation is known as bone mineralization. Basically, it is a process of deposition of minerals on the bone matrix for the growth and development of the bone [6]. Disease that can cause disorders of bone mineralization in children includes rickets, renal disease, and tumour-induced osteomalacia. The core idea of studying the mathematical model for bone mineralization is to know more about how to solve this numerically in order to forecast the reaction of the system, which could result in major clinical signs like bone abnormalities and fractures. In this article, we have studied the mathematical model of the

bone mineralization process, which is described in detail by Komarova [11] and the references cited therein.

Attempts have been made to do quantitative formulation in terms of mathematical laws that relate the mineralization process with predefined parameters. Furthermore, it is explained how this mineralization is measured together with the mathematical formulation of the model and how this can be influenced by several impacts. This helps us to deal with bone diseases and drug therapies. For a fruitful interplay between theory and simulation, considerable efforts have been made to make both outputs comparable. We validate the accuracy of model predictions using bone diseases associated with dramatic changes in mineralization dynamics due to key parameters.

2.1 Mathematical Model

An important and effective way to understand the biological problems is by establishing the mathematical models and analyzing their dynamical behaviors. Various types of mathematical models of biological processes were discussed previously by many authors (see, e.g. [4, 9, 10, 14]). In the present framework, we consider the model for bone mineralization that was given by Komarova [11]. The following system of equations describes the dynamics of bone mineralization:

$$\frac{d\mathbf{x}_1}{dt} = -k_1\mathbf{x}_1, \tag{7}$$

$$\frac{d\mathbf{x}_2}{dt} = k_1\mathbf{x}_1, \tag{8}$$

$$\frac{d\mathfrak{J}}{dt} = v_1\mathbf{x}_1 - r_1\mathbf{x}_2\mathfrak{J}, \tag{9}$$

$$\frac{d\mathfrak{N}}{dt} = k_2\frac{d\mathbf{x}_2}{dt} - r_2\frac{d\eta}{dt}\mathfrak{N}, \tag{10}$$

$$\frac{d\eta}{dt} = k_3\left(\frac{\rho}{\rho + \mathfrak{J}^\sigma}\right)\mathfrak{N}. \tag{11}$$

The notations and various terms of the equations used in the model are as follows:

\mathbf{x}_1 : Concentration of naive collagen.

\mathbf{x}_2 : Concentration of mature collagen.

\mathfrak{J} : Inhibitor of mineralization.

\mathfrak{N} : Number of the nucleators that help in the process of mineralization and act on mature collagen.

η : Mineral

k_1 : It is the rate at which collagen cross-linking takes place and is inversely related to time lag.

The relationships are defined by the equations (7) and (8), and the collagen matrix is created from raw osteoblasts (bone-forming cells) that develop into fully constructed collagen matrix (\mathbf{x}_2).

v_1 : It refers to the rate at which inhibitors permeate through immature collagen and into the extracellular compartment close to the cells. It has an inverse relationship with time and directly influences the maximum value of \mathfrak{J} . As a result,

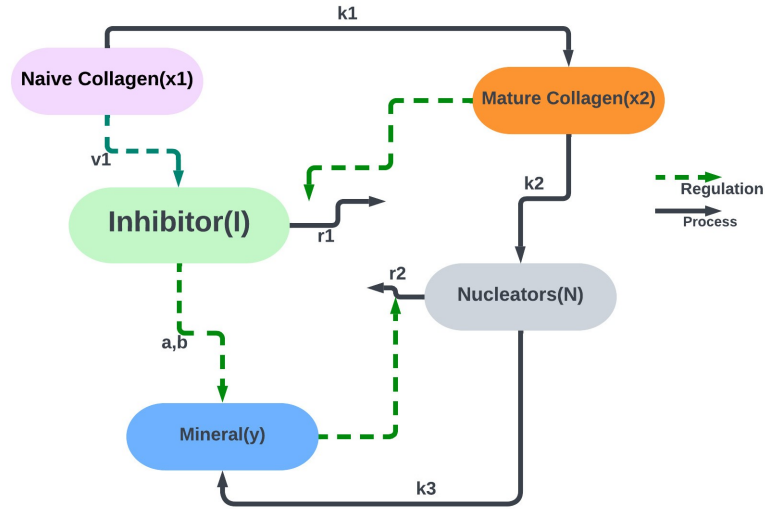


Figure 1: Schematic representation of the model dynamics for bone mineralization.

the amount of inhibitor is proportional to the availability of naive or raw collagen, as indicated by the term v_1x_1 .

The idea is to stimulate the mature collagen because naive collagen can not be mineralized. Inhibitor prevent the conversion of the naive collagen into mature collagen.

r_1 : It is the rate by which the inhibitor removal or reduction takes place.

In equation (9), $r_1x_2\mathcal{I}$ represents reduction of inhibitors with rate constant r_1 and is induced by the involvement of mature collagen x_2 .

k_2 : The number of nucleators present in each mature collagen molecule.

Each collagen molecule has only one intrafibrillar nucleator when $k_2 = 1$, although interfibrillar nucleators behave similarly.

There is a mixture of intrafibrillar and interfibrillar nucleators when $k_2 \geq 1$. As a result, the rate of nucleator appearance, which is proportional to matrix maturation, is represented by $k_2 \frac{dx_2}{dt}$.

r_2 : It is the rate by which mineral mask the nucleator. The number of nucleators diminishes as the mineral covers them up when a certain nucleator starts the mineralization. The rate of decrease of nucleators in equation (10), is thought to be proportional to both the concentration of nucleators present and the rate at which mineralized crystals emerge i.e. $\frac{d\eta}{dt}$.

k_3 : The rate at which mineralization takes place.

From a physiological perspective, the process of forming bone tissues starts when osteoblasts secrete an organic bone matrix made up of collagen. This raw collagen matrix must be treated to accommodate mineralization once it is deposited into the extracellular compartment; this process is known as matrix maturation.

This model and its simulations have been done by considering the following assumptions:

1. Nucleators generated during collagen maturation are eliminated from the

system in proportion to the rate of mineralization.

2. The model does not define the elaborate process of matrix maturation.
3. Different types of inhibitors are utilized, but they are treated as a single entity.
4. Similarly, interfibrillar and intrafibrillar nucleators are not properly distinguished.

The analysis and observations of the model may help us to find the cure for numerous bone-related diseases like Osteogenesis imperfecta (OI), which is usually caused due to increased bone mineralization resulting in high bone fragility, low bone mass, and brittleness of bones. Mathematically, it can be interpreted as increase in mineralization degree and a decrease in mineralization lag time which has been explained in later sections of this paper through graphical representation. Osteomalacia and Osteoporosis are disease that are caused by to decrease in the degree of bone mineralization and low mineral content respectively.

3 Fractional bone mineralization model

Recently, in the chapter [1], the authors have studied the qualitative analysis and numerical simulation of the integer order model defined by (7)– (11).

Since the recent research involving the fractional-order derivatives has produced superior results in simulating real-world occurrences, we investigate the process of bone mineralization using the Caputo fractional-order derivative. The fractional-order derivative is the generalization of the integer-order derivative and is capable of carrying the memory of the system. It is also helpful in the detection of any lag in the process. Motivated by the work in the field of fractional modeling, we moderate this dynamical system by substituting the time derivative with the Caputo-fractional time derivative.

On fractionalizing the model (7)- (11) using the Caputo fractional derivative of order $0 < \alpha \leq 1$, we get

$${}_0^C D_t^\alpha \mathfrak{x}_1 = -k_1^\alpha \mathfrak{x}_1, \tag{12}$$

$${}_0^C D_t^\alpha \mathfrak{x}_2 = k_1^\alpha \mathfrak{x}_1, \tag{13}$$

$${}_0^C D_t^\alpha \mathfrak{J} = v_1^\alpha \mathfrak{x}_1 - r_1^\alpha \mathfrak{x}_2 \mathfrak{J}, \tag{14}$$

$${}_0^C D_t^\alpha \mathfrak{N} = k_2 ({}_0^C D_t^\alpha \mathfrak{x}_2) - r_2 ({}_0^C D_t^\alpha \mathfrak{N}), \tag{15}$$

$${}_0^C D_t^\alpha \mathfrak{N} = k_3^\alpha \left(\frac{\rho}{\rho + \mathfrak{J}^\sigma} \right) \mathfrak{N}. \tag{16}$$

The ordinary derivative has an inverse second dimension s^{-1} and the fractional derivative has a dimension of $s^{-\alpha}$. For the non-dimensionlization, making the substitutions

$$X_1 = \frac{\mathfrak{x}_1}{\hat{\mathfrak{x}}_1}, X_2 = \frac{\mathfrak{x}_2}{\hat{\mathfrak{x}}_2}, Y = \frac{\mathfrak{N}}{\hat{\mathfrak{N}}}, \tilde{I} = \frac{\mathfrak{J}}{\hat{\mathfrak{I}}}, \tilde{N} = \frac{\mathfrak{N}}{\hat{\mathfrak{N}}}, r_1^\alpha \hat{\mathfrak{x}}_1 = \hat{r}_1, r_2 \hat{\mathfrak{N}} = \hat{r}_2, \hat{b} = \frac{b}{\hat{\mathfrak{x}}_1^a}, \frac{k_3^\alpha \hat{\mathfrak{x}}_1}{\hat{\mathfrak{N}}} =$$

$\hat{k}_3, k_1^\alpha = \hat{k}_1, v_1^\alpha = \hat{v}_1, \hat{x}_1 = \hat{x}_2 = 10^6 \text{molecules}/\mu\text{m}^3, \eta_1 = 10^9 \text{molecules}/\mu\text{m}^3$ in the system (12)-(16), it gets transformed into:

$${}_0^C D_t^\alpha X_1 = -\hat{k}_1 X_1, \tag{17}$$

$${}_0^C D_t^\alpha X_2 = \hat{k}_1 X_1, \tag{18}$$

$${}_0^C D_t^\alpha \tilde{I} = \hat{v}_1 X_1 - \hat{r}_1 X_2 \tilde{I}, \tag{19}$$

$${}_0^C D_t^\alpha \tilde{N} = k_2 ({}_0^C D_t^\alpha X_2) - \hat{r}_2 ({}_0^C D_t^\alpha Y) \tilde{N}, \tag{20}$$

$${}_0^C D_t^\alpha Y = \hat{k}_3 \left(\frac{\tilde{\rho}}{\tilde{\rho} + \tilde{I}^\sigma} \right) \tilde{N}. \tag{21}$$

For this fractional model, we perform the qualitative analysis i.e. the existence and uniqueness of the solution of the defined coupled system is proved. The model is simulated for observing the behavior of the variable under the impact of fractional order derivative. A comparison with integer order derivative helps in understanding the phenomenon in a better way. The sensitivity analysis for the fractional model is done with respect to the parameters of the model.

4 Qualitative analysis of the model

In this section, the qualitative analysis of the model has been done. We shall first prove the existence and uniqueness of the solution of the system (17)-(21). The existence and uniqueness of the solution are the key ideas in the field of differential equations as they ensure that a solution to the fractional order model exists and can be found by one or the other method. It also guarantees that if the solution exists, it is unique.

4.1 Existence and Uniqueness of Solution

If $C(J)$ is the collection of continuous real-valued functions defined on the interval $J \subset R$. Then $V = C(J) * C(J) * C(J) * C(J) * C(J)$ is the Banach space with the norm for $(X_1, X_2, \tilde{I}, \tilde{N}, Y) \in V$ defined as $\|(X_1, X_2, \tilde{I}, \tilde{N}, Y)\| = \|X_1\| + \|X_2\| + \|\tilde{I}\| + \|\tilde{N}\| + \|Y\|$, where $X_1, X_2, \tilde{I}, \tilde{N}, Y \in C(J)$ and $\|\cdot\| = \sup_{t \in J} |\cdot|$. With the application of the fixed point theorem, we shall prove that the solution of the system of differential equations (17)-(21) exists.

Applying the integral operator (5) upon the equation (17),

$$I_t^\alpha {}_0^C D_t^\alpha X_1 = I_t^\alpha (-\hat{k}_1 X_1), \tag{22}$$

we obtain

$$X_1(t) - X_1(0) = \frac{1}{\Gamma(\alpha)} \int_0^t (t - \tau)^{\alpha-1} (-\hat{k}_1 X_1(\tau)) d\tau. \tag{23}$$

Similarly,

$$X_2(t) - X_2(0) = \frac{1}{\Gamma(\alpha)} \int_0^t (t - \tau)^{\alpha-1} (\hat{k}_1 X_1(\tau)) d\tau, \tag{24}$$

$$\tilde{I}(t) - \tilde{I}(0) = \frac{1}{\Gamma(\alpha)} \int_0^t (t - \tau)^{\alpha-1} (\hat{v}_1 X_1 - \hat{r}_1 X_2 \tilde{I}) d\tau, \tag{25}$$

$$\tilde{N}(t) - \tilde{N}(0) = \frac{1}{\Gamma(\alpha)} \int_0^t (t - \tau)^{\alpha-1} (k_2 \hat{k}_1 X_1 - \hat{r}_2 ({}^C D_t^\alpha Y) \tilde{N}) d\tau, \tag{26}$$

$$Y(t) - Y(0) = \frac{1}{\Gamma(\alpha)} \int_0^t (t - \tau)^{\alpha-1} \left(\hat{k}_3 \left(\frac{\tilde{\rho}}{\tilde{\rho} + \tilde{I}^\sigma} \right) \tilde{N} \right) d\tau. \tag{27}$$

Denote,

$$\begin{aligned} \mathcal{K}_1 &= -\hat{k}_1 X_1, \\ \mathcal{K}_2 &= \hat{k}_1 X_1, \\ \mathcal{K}_3 &= \hat{v}_1 X_1 - \hat{r}_1 X_2 \tilde{I}, \\ \mathcal{K}_4 &= k_2 ({}^C D_t^\alpha X_2) - \hat{r}_2 ({}^C D_t^\alpha Y) \tilde{N}, \\ \mathcal{K}_5 &= \hat{k}_3 \left(\frac{\tilde{\rho}}{\tilde{\rho} + \tilde{I}^\sigma} \right) \tilde{N}. \end{aligned} \tag{28}$$

The kernels $\mathcal{K}_i, i = 1, 2, 3, 4, 5$ satisfy certain requirements, as stated in the following theorem [2].

Theorem 4.1. *The Lipschitz condition and contraction would be satisfied by $\mathcal{K}_1, \mathcal{K}_2, \mathcal{K}_3, \mathcal{K}_4, \mathcal{K}_5$, for the Lipschitz constants $0 \leq \hat{k}_1 < 1, 0 \leq \hat{r}_1 c_1 < 1, 0 \leq 2\hat{r}_2 k_2 \hat{k}_3 c_1 < 1$.*

Proof. Let us start with \mathcal{K}_1 . Let X_1 and $X_1^{(1)}$ are two functions, then

$$\begin{aligned} \|\mathcal{K}_1(t, X_1) - \mathcal{K}_1(t, X_1^{(1)})\| &= \| -\hat{k}_1 X_1 + \hat{k}_1 X_1^{(1)} \| \\ &= \hat{k}_1 \|X_1 - X_1^{(1)}\|. \end{aligned} \tag{29}$$

Clearly, \hat{k}_1 is a fixed parameter and $\|X_1\|$ is a bounded function.

Hence the Lipschitz condition is satisfied for \mathcal{K}_1 , and it is contraction mapping.

Similarly, the other four kernels also satisfy the Lipschitz condition, i.e.,

$$\begin{aligned} \|\mathcal{K}_2(t, X_2) - \mathcal{K}_2(t, X_2^{(1)})\| &= \hat{k}_1 \|X_2 - X_2^{(1)}\|, \\ \|\mathcal{K}_3(t, \tilde{I}) - \mathcal{K}_3(t, \tilde{I}^{(1)})\| &= \hat{r}_1 c_1 \|\tilde{I} - \tilde{I}^{(1)}\|, \\ \|\mathcal{K}_4(t, \tilde{N}) - \mathcal{K}_4(t, \tilde{N}^{(1)})\| &= 2\hat{r}_2 k_2 \hat{k}_3 c_1 \|\tilde{N} - \tilde{N}^{(1)}\|, \\ \|\mathcal{K}_5(t, Y) - \mathcal{K}_5(t, Y^{(1)})\| &= 0, \end{aligned} \tag{30}$$

On using the above kernels from (28) in the equations (23) - (27), we get

$$\begin{aligned} X_1(t) &= X_1(0) + \int_0^t \mathcal{K}_1(\tau, X_1(\tau)) d\tau, \\ X_2(t) &= X_2(0) + \int_0^t \mathcal{K}_2(\tau, X_2(\tau)) d\tau, \\ \tilde{I}(t) &= \tilde{I}(0) + \int_0^t \mathcal{K}_3(\tau, \tilde{I}(\tau)) d\tau, \\ \tilde{N}(t) &= \tilde{N}(0) + \int_0^t \mathcal{K}_4(\tau, \tilde{N}(\tau)) d\tau, \\ Y(t) &= Y(0) + \int_0^t \mathcal{K}_5(\tau, Y(\tau)) d\tau. \end{aligned} \tag{31}$$

Corresponding recursive formulas are given by

$$\begin{aligned}
 X_1^{(n)}(t) &= \int_0^t \mathcal{K}_1(\tau, X_1^{(n-1)}(\tau))d\tau, \\
 X_2^{(n)}(t) &= \int_0^t \mathcal{K}_2(\tau, X_2^{(n-1)}(\tau))d\tau, \\
 \tilde{I}^{(n)}(t) &= \int_0^t \mathcal{K}_3(\tau, \tilde{I}^{(n-1)}(\tau))d\tau, \\
 \tilde{N}^{(n)}(t) &= \int_0^t \mathcal{K}_4(\tau, \tilde{N}^{(n-1)}(\tau))d\tau, \\
 Y^{(n)}(t) &= \int_0^t \mathcal{K}_5(\tau, Y^{(n-1)}(\tau))d\tau.
 \end{aligned} \tag{32}$$

The initial conditions are $X_1^{(0)} = X_1(0), X_2^{(0)} = X_2(0), \tilde{I}^{(0)} = \tilde{I}(0), \tilde{N}^{(0)} = \tilde{N}(0), Y^{(0)} = Y(0)$.

The following expressions represent respectively the difference of the terms in (32) with their succeeding terms,

$$\begin{aligned}
 \psi_{1n}(t) &= X_1^{(n)}(t) - X_1^{(n-1)}(t) \\
 &= \frac{1}{\Gamma(\alpha)} \int_0^t (\mathcal{K}_1(\tau, X_1^{(n-1)}(\tau)) - \mathcal{K}_1(\tau, X_1^{(n-2)}(\tau)))(x - \tau)^{\alpha-1} d\tau,
 \end{aligned} \tag{33}$$

$$\begin{aligned}
 \psi_{2n}(t) &= X_2^{(n)}(t) - X_2^{(n-1)}(t) \\
 &= \frac{1}{\Gamma(\alpha)} \int_0^t (\mathcal{K}_2(\tau, X_2^{(n-1)}(\tau)) - \mathcal{K}_2(\tau, X_2^{(n-2)}(\tau)))(x - \tau)^{\alpha-1} d\tau,
 \end{aligned} \tag{34}$$

$$\begin{aligned}
 \psi_{3n}(t) &= \tilde{I}^{(n)}(t) - \tilde{I}^{(n-1)}(t) \\
 &= \frac{1}{\Gamma(\alpha)} \int_0^t (\mathcal{K}_3(\tau, \tilde{I}^{(n-1)}(\tau)) - \mathcal{K}_3(\tau, \tilde{I}^{(n-2)}(\tau)))(x - \tau)^{\alpha-1} d\tau,
 \end{aligned} \tag{35}$$

$$\begin{aligned}
 \psi_{4n}(t) &= \tilde{N}^{(n)}(t) - \tilde{N}^{(n-1)}(t) \\
 &= \frac{1}{\Gamma(\alpha)} \int_0^t (\mathcal{K}_4(\tau, \tilde{N}^{(n-1)}(\tau)) - \mathcal{K}_4(\tau, \tilde{N}^{(n-2)}(\tau)))(x - \tau)^{\alpha-1} d\tau,
 \end{aligned} \tag{36}$$

$$\begin{aligned}
 \psi_{5n}(t) &= Y^{(n)}(t) - Y^{(n-1)}(t) \\
 &= \frac{1}{\Gamma(\alpha)} \int_0^t (\mathcal{K}_5(\tau, Y^{(n-1)}(\tau)) - \mathcal{K}_5(\tau, Y^{(n-2)}(\tau)))(x - \tau)^{\alpha-1} d\tau.
 \end{aligned} \tag{37}$$

Now, on taking norm of (33),

$$\begin{aligned}
 |\psi_{1n}(t)| &= \left\| X_1^{(n)}(t) - X_1^{(n-1)}(t) \right\| \\
 &= \left\| \frac{1}{\Gamma(\alpha)} \int_0^t (\mathcal{K}_1(\tau, X_1^{(n-1)}(\tau)) - \mathcal{K}_1(\tau, X_1^{(n-2)}(\tau)))d\tau \right\| \\
 &\leq \int_0^t \left\| (\mathcal{K}_1(\tau, X_1^{(n-1)}(\tau)) - \mathcal{K}_1(\tau, X_1^{(n-2)}(\tau))) \right\| d\tau.
 \end{aligned} \tag{38}$$

As the kernel \mathcal{K}_1 fulfill the Lipschitz condition, we have

$$\|X_1^{(n)}(t) - X_1^{(n-1)}(t)\| \leq \hat{k}_1 \int_0^t \|X_1^{(n-1)}(t) - X_1^{(n-2)}(t)\| d\tau, \tag{39}$$

and hence,

$$\|\psi_{1n}(t)\| \leq \gamma_1 \int_0^t \|\psi_{1(n-1)}(t)(\tau)\| d\tau. \tag{40}$$

Similarly,

$$\|\psi_{2n}(t)\| \leq \gamma_2 \int_0^t \|\psi_{2(n-1)}(\tau)\| d\tau, \tag{41}$$

$$\|\psi_{3n}(t)\| \leq \gamma_3 \int_0^t \|\psi_{3(n-1)}(\tau)\| d\tau, \tag{42}$$

$$\|\psi_{4n}(t)\| \leq \gamma_4 \int_0^t \|\psi_{4(n-1)}(\tau)\| d\tau, \tag{43}$$

$$\|\psi_{5n}(t)\| \leq \gamma_5 \int_0^t \|\psi_{5(n-1)}(\tau)\| d\tau, \tag{44}$$

where, $\gamma_1 = \gamma_2 = \hat{k}_1$, $\gamma_3 = \hat{r}_1 c_1$, $\gamma_4 = 2\hat{r}_2 k_2 \hat{k}_3 c_1$, $\gamma_5 = 0$.

Hence,

$$X_1^{(n)}(t) = \sum_{i=0}^n \psi_{1n}(t), \tag{45}$$

$$X_2^{(n)}(t) = \sum_{i=0}^n \psi_{2n}(t), \tag{46}$$

$$\tilde{I}^{(n)}(t) = \sum_{i=0}^n \psi_{3n}(t), \tag{47}$$

$$\tilde{N}^{(n)}(t) = \sum_{i=0}^n \psi_{4n}(t), \tag{48}$$

$$Y^{(n)}(t) = \sum_{i=0}^n \psi_{5n}(t). \tag{49}$$

□

In the following theorem we prove the existence and uniqueness of the solution [12].

Theorem 4.2. *The system of fractional bone mineralization model has an exact coupled solution under the condition that we can find t_1 such that $\frac{\hat{k}_1 t_1}{\Gamma(\alpha)} \leq$*

1, $\frac{\hat{r}_1 c_1 t_1}{\Gamma(\alpha)} \leq 1$, $\frac{\hat{r}_2 \hat{k}_3 t}{\Gamma(\alpha)} \leq 1$ and also the solution is unique.

Proof. The functions $X_1(t)$, $X_2(t)$, $\tilde{I}(t)$, $\tilde{N}(t)$, and $Y(t)$ are bounded and the Lipschitz condition is satisfied by the kernels \mathcal{K}_i , $i = 1, 2, 3, 4, 5$,

$$\begin{aligned} X_1(t) - X_1(0) &= X_1^{(n)}(t) - \mathcal{H}_1^{(n)}(t), \\ X_2(t) - X_2(0) &= X_2^{(n)}(t) - \mathcal{H}_2^{(n)}(t), \\ \tilde{I}(t) - \tilde{I}(0) &= \tilde{I}^{(n)}(t) - \mathcal{H}_3^{(n)}(t), \\ \tilde{N}(t) - \tilde{N}(0) &= \tilde{N}^{(n)}(t) - \mathcal{H}_4^{(n)}(t), \\ Y(t) - Y(0) &= Y^{(n)}(t) - \mathcal{H}_5^{(n)}(t). \end{aligned} \tag{50}$$

Now,

$$\begin{aligned} \mathcal{H}_1^{(n)}(t) &= X_1^{(n)}(t) - X_1(t) + X_1(0) \\ \implies \|\mathcal{H}_1^{(n)}(t)\| &= \left\| \frac{1}{\Gamma(\alpha)} \int_0^t \mathcal{K}_1(\tau, X_1^{(n-1)}(\tau))d\tau - X_1(t) + X_1(0) \right\| \\ &= \frac{1}{\Gamma(\alpha)} \left\| \int_0^t \mathcal{K}_1(\tau, X_1^{(n-1)}(\tau))d\tau + X_1(0) - X_1(t) - \int_0^t \mathcal{K}_1(\tau, X_1(\tau))d\tau \right\| \\ &= \frac{1}{\Gamma(\alpha)} \int_0^t \|(\mathcal{K}_1(\tau, X_1^{(n-1)}(\tau)) - \mathcal{K}_1(\tau, X_1(\tau)))\|d\tau \\ &\leq \frac{\hat{k}_1}{\Gamma(\alpha)} \|X_1^{(n-1)} - X_1\| \int_0^t d\tau \\ &\leq \frac{\hat{k}_1}{\Gamma(\alpha)} \|X_1^{(n-1)} - X_1\|t. \end{aligned} \tag{51}$$

On repeated use of above process, we get

$$\|\mathcal{H}_1^{(n)}(t)\| \leq (\hat{k}_1)^{n+1} \left(\frac{t}{\Gamma(\alpha)}\right)^{n+1} \lambda. \tag{52}$$

Thus, $\exists t_1$ such that

$$\|\mathcal{H}_1^{(n)}(t)\| \leq (\hat{k}_1)^{n+1} \left(\frac{t_1}{\Gamma(\alpha)}\right)^{n+1} \lambda. \tag{53}$$

Taking the limit $n \rightarrow \infty$, since, $0 \leq \hat{k}_1 t < 1$,

$$\|\mathcal{H}_1^{(n)}(t)\| \rightarrow 0. \implies X_1(t) - X_1(0) = \lim_{n \rightarrow \infty} X_1^{(n)}(t) \tag{54}$$

Similarly,

$$\begin{aligned} \|\mathcal{H}_2^{(n)}(t)\| &\leq \frac{\hat{k}_1 t}{\Gamma(\alpha)} \|X_2^{(n-1)} - X_2\| \\ \|\mathcal{H}_3^{(n)}(t)\| &\leq \frac{\hat{r}_1 c_1 t}{\Gamma(\alpha)} \|\tilde{I}^{(n-1)} - \tilde{I}\| \\ \|\mathcal{H}_4^{(n)}(t)\| &\leq \frac{\hat{r}_2 \hat{k}_3 t}{\Gamma(\alpha)} \|\tilde{N}^{(n-1)} - \tilde{N}\| \\ \|\mathcal{H}_5^{(n)}(t)\| &= 0, \end{aligned} \tag{55}$$

and hence, we have

$$\begin{aligned}
 \|\mathcal{H}_2^{(n)}(t)\| \rightarrow 0. & \implies X_2(t) - X_2(0) = \lim_{n \rightarrow \infty} X_2^{(n)}(t), \\
 \|\mathcal{H}_3^{(n)}(t)\| \rightarrow 0. & \implies \tilde{I}(t) - \tilde{I}(0) = \lim_{n \rightarrow \infty} \tilde{I}^{(n)}(t), \\
 \|\mathcal{H}_4^{(n)}(t)\| \rightarrow 0. & \implies \tilde{N}(t) - \tilde{N}(0) = \lim_{n \rightarrow \infty} \tilde{N}^{(n)}(t), \\
 \|\mathcal{H}_5^{(n)}(t)\| \rightarrow 0. & \implies Y(t) - Y(0) = \lim_{n \rightarrow \infty} Y^{(n)}(t).
 \end{aligned} \tag{56}$$

This proves that the solution to the given system exists.

To prove that the solution is unique, let us assume that $X'_1, X'_2, \tilde{I}', \tilde{N}', Y'$ be another set of solutions of the system (7)-(11). Then from (32)

$$\begin{aligned}
 X_1(t) - X'_1(t) &= \int_0^t (\mathcal{K}_1(\tau, X_1) - \mathcal{K}_1(\tau, X'_1))d\tau \\
 \implies \|X_1(t) - X'_1(t)\| &\leq \hat{k}_1 t \|X_1(t) - X'_1(t)\| \\
 \implies \|X_1(t) - X'_1(t)\| &= 0 \quad \text{since } \hat{k}_1 t < 1 \\
 \implies X_1(t) &= X'_1(t).
 \end{aligned} \tag{57}$$

Uniqueness can be proved for the other variables $X_2, \tilde{I}, \tilde{N}, Y$ in the similar way. \square

4.2 Stability Analysis

Since the system of equations is a model of the physical behavior of the simulation's objects, the stability of the system of differential equations is defined as the physical stability of the system. In the model (17) – (21), defining the functions as follows

$$f_1 = -\hat{k}_1 X_1, \tag{58}$$

$$f_2 = \hat{k}_1 X_1, \tag{59}$$

$$f_3 = \hat{v}_1 X_1 - \hat{r}_1 X_2 \tilde{I}, \tag{60}$$

$$f_4 = k_2 \left({}^C D_t^\alpha \right) X_2 - \hat{r}_2 \left({}^C D_t^\alpha \right) Y \tilde{N}, \tag{61}$$

$$f_5 = \hat{k}_3 \left(\frac{\tilde{\rho}}{\tilde{\rho} + \tilde{I}^\sigma} \right) \tilde{N}. \tag{62}$$

The critical points will be obtained for $f_i=0, i = 1, 2, 3, 4, 5$.

$$f_1 = -\hat{k}_1 X_1 = 0 \implies X_1 = 0$$

Since, $X_1 + X_2 = K$, we have $X_2 = K$. Now,

$$f_3 = \hat{v}_1 X_1 - \hat{r}_1 X_2 \tilde{I} = 0 \implies \hat{v}_1 X_1 - \hat{r}_1 K \tilde{I} = 0 \implies \tilde{I} = 0.$$

Also,

$$f_5 = \hat{k}_3 \left(\frac{\tilde{\rho}}{\tilde{\rho} + \tilde{I}^\sigma} \right) \tilde{N} = 0 \implies \tilde{N} = 0.$$

$$f_4 = k_2 \hat{k}_1 X_1 - \hat{r}_2 ({}^C D_t^\alpha Y) \tilde{N} = 0 \implies \hat{r}_2 ({}^C D_t^\alpha Y) \tilde{N} = 0.$$

${}^C D_t^\alpha Y$ may or may not be zero. Hence, the system has infinitely many critical points $(X_1, X_2, \tilde{I}, \tilde{N}, Y) = (0, K, 0, 0, Y)$.

Now, we will check whether the given system is stable or unstable at the critical points. So, for this, we will find the Jacobian matrix.

The general form of the Jacobian matrix for the given system of bone mineralization will be:

$$J = \frac{\partial(f_1, f_2, f_3, f_4, f_5)}{\partial(X_1, X_2, \tilde{I}, \tilde{N}, Y)} = \begin{bmatrix} \frac{\partial f_1}{\partial X_1} & \frac{\partial f_1}{\partial X_2} & \frac{\partial f_1}{\partial \tilde{I}} & \frac{\partial f_1}{\partial \tilde{N}} & \frac{\partial f_1}{\partial Y} \\ \frac{\partial f_2}{\partial X_1} & \frac{\partial f_2}{\partial X_2} & \frac{\partial f_2}{\partial \tilde{I}} & \frac{\partial f_2}{\partial \tilde{N}} & \frac{\partial f_2}{\partial Y} \\ \frac{\partial f_3}{\partial X_1} & \frac{\partial f_3}{\partial X_2} & \frac{\partial f_3}{\partial \tilde{I}} & \frac{\partial f_3}{\partial \tilde{N}} & \frac{\partial f_3}{\partial Y} \\ \frac{\partial f_4}{\partial X_1} & \frac{\partial f_4}{\partial X_2} & \frac{\partial f_4}{\partial \tilde{I}} & \frac{\partial f_4}{\partial \tilde{N}} & \frac{\partial f_4}{\partial Y} \\ \frac{\partial f_5}{\partial X_1} & \frac{\partial f_5}{\partial X_2} & \frac{\partial f_5}{\partial \tilde{I}} & \frac{\partial f_5}{\partial \tilde{N}} & \frac{\partial f_5}{\partial Y} \end{bmatrix}. \tag{63}$$

Substituting for $f_i, i = 1, 2, 3, 4, 5$ in the matrix, we get the following Jacobian Matrix:

$$\begin{bmatrix} -\hat{k}_1 & 0 & 0 & 0 & 0 \\ \hat{k}_1 & 0 & 0 & 0 & 0 \\ \hat{v}_1 & -\hat{r}_1 \tilde{I} & 0 & 0 & 0 \\ \hat{k}_1 k_2 & 0 & 0 & 0 & 0 \\ 0 & 0 & 0 & \frac{\hat{k}_3 \tilde{\rho}}{\tilde{\rho} + \tilde{I}^\sigma} & 0 \end{bmatrix}. \tag{64}$$

The eigen values corresponding to above matrix are $0, 0, 0, -\hat{k}_1, -\hat{k}_1 \hat{r}_1$. Observing the eigenvalues, we can conclude that the system is *marginally stable* at the critical points $(0, K, 0, 0, Y)$, which occur after a short span of time period just after the start of the mineralization process. Thus, the mineralization will not suddenly explode and the system will always have bounded solution but no steady state output.

5 Simulation and discussion

The numerical simulation has been done using the Lagrange’s two-step method . Applying Lagrange’s two-step method for the Caputo fractional derivative [3, Eq.

2.89], we get the following numerical scheme for (23).

$$\begin{aligned}
 X_1(n+1) &= X_1(1) + \frac{h^\alpha}{\Gamma(\alpha+2)} \\
 &\times \left(\sum_{k=2}^n [(n-k+1)^\alpha(n-k+2+\alpha) - (n-k)^\alpha(n-k+2+2\alpha)] f(t(k), X_1(k)) \right. \\
 &\left. - \sum_{k=2}^n [(n-k+1)^{\alpha+1} - (n-k)^\alpha(n-k+1+\alpha)] f(t(k-1), X_1(k-1)) \right) \tag{65}
 \end{aligned}$$

Similarly, expression for other variables $X_2, \tilde{I}, \tilde{N}, Y$ can be obtained. The values of the parameters are mentioned in Table 1 as provided in [11] and are used for the purpose of simulation. These values are relevant to the mineralization process in human bone and also agree with the theoretical analysis of human disorders of bone mineralization.

Table 1: Model parameters

Parameter	Description	Value
k_1	Collagen cross-linking rate	0.1/ day
k_2	Nucleator count per collagen molecule	1
k_3	rate of mineral formation of mineral	1000/day
r_1	rate of inhibitors degradation	2×10^{-7} /day
v_1	rate of production of inhibitors by osteoblasts	0.1 per day
r_2	nucleators covered by mineral	1.7×10^{-8} /mol
σ	Hill coefficient	10
ρ	Hill function parameter	10^{57}

The plots are created for different values of the order α of the Caputo fractional operator. In Figure 2, it is observed that raw collagen, which initially constituted 100 percent of the total collagen in the system, decreases with the passage of time as it gets converted into mature collagen. The figure explores the temporal change of concentration of raw collagen for different values of α and shows a similar pattern with integer order suggesting that the fractional order model is well-posed, effective, and precise.

Figure 3 explores the temporal change of mature collagen for different values of α . which leads to 70 – 80 percent conversion in 20 days and complete maturation in 45 – 60 days. Figure 4 depicts the impact of inhibitors for different values of α . Inhibitors were initially present in raw collagen frameworks for 10 days before being rapidly destroyed with the development of mature collagen.

Figure 5 depicts the impact of nucleators for different values of α with respect to time. As the process gets started and paces up nucleator distribution into the system is sluggish. Figure 6 depicts the impact of mineralization for different values of α and graph also shows the lag time which is required for mineralization which is approximately 10 days and mineralization then gradually increases with

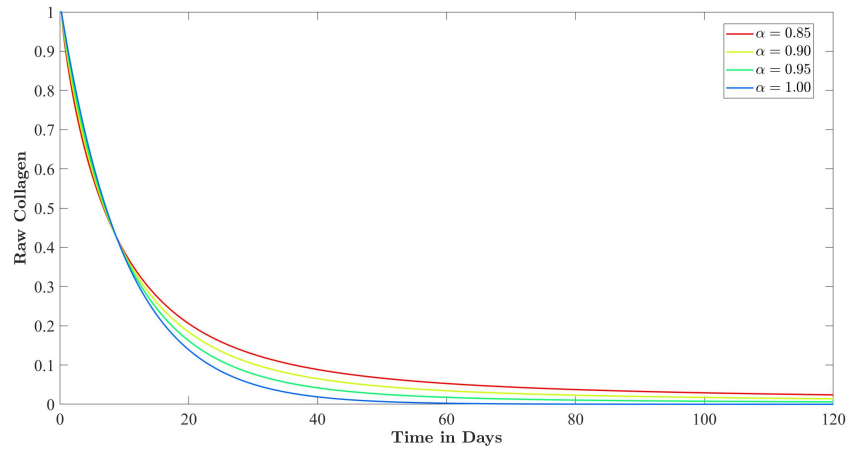


Figure 2: Variation in raw collagen with time for different value of $\alpha = 0.85, 0.90, 0.95, 1$.

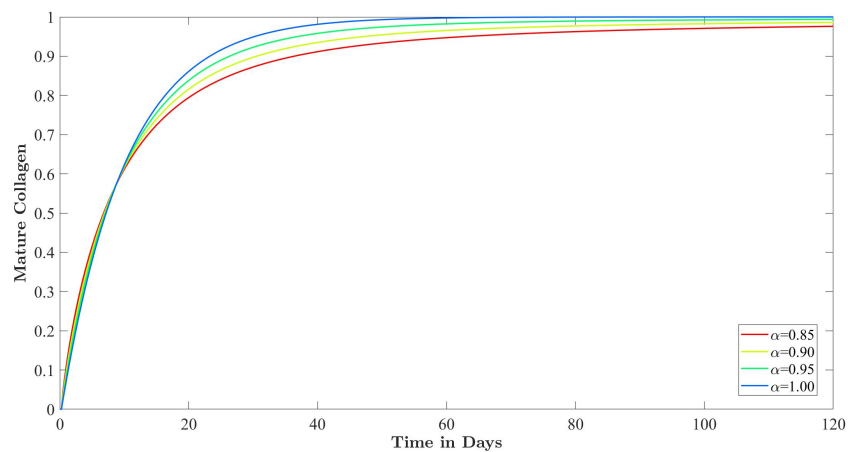


Figure 3: Variation in mature collagen with time for different values of $\alpha = 0.85, 0.90, 0.95, 1$.

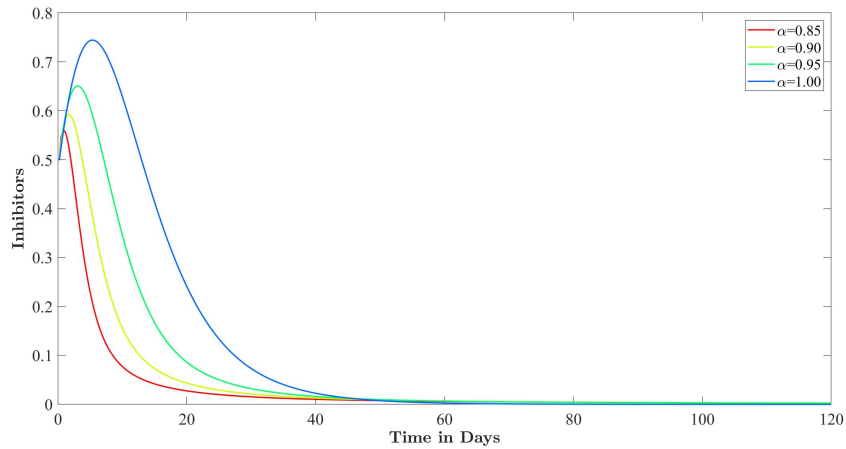


Figure 4: Variation in inhibitors with time for different value of $\alpha = 0.85, 0.90, 0.95, 1$.

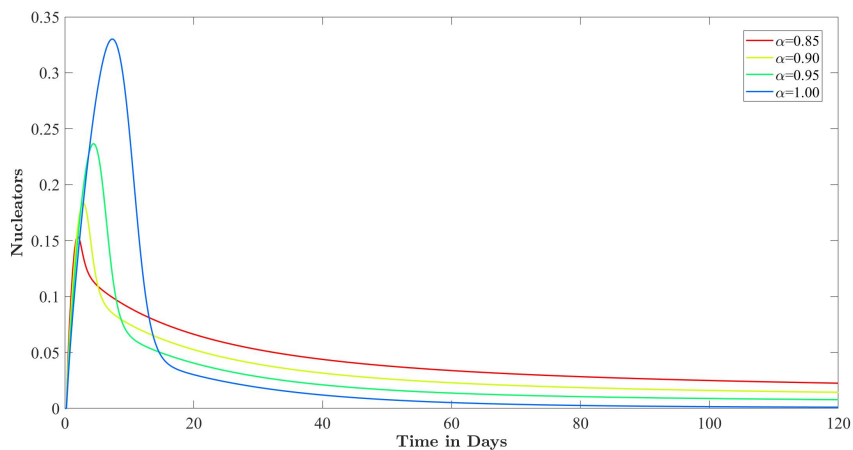


Figure 5: Variation in the nucleator quantity with time for different value of $\alpha = 0.85, 0.90, 0.95, 1$.

time. The normalized mineralization degree of 1 is attained in 100 days after the deposition of raw collagen takes place.

The graphs plotted provide the variation in the values of the variable when the values of α are changed. The value of the order α of fractional derivative can be chosen to fit the experimental data, if available.

Mineralization lag time is the amount of time required to start the mineralization process. In a healthy human bone, it takes approximately 10 days. After the lag was completed mineralization began quickly, followed by a steady decline in mineral formation whereas, the mineralization degree is the greatest amount of mineralization that may occur. The normalized mineralization degree of 1 (i.e., full mineralization) was obtained 100 days after the deposition of raw collagen. It is further observed from Figure 6 that, the fractional model can help in detecting any anomaly in mineralization at an early stage compared to the integer order model.

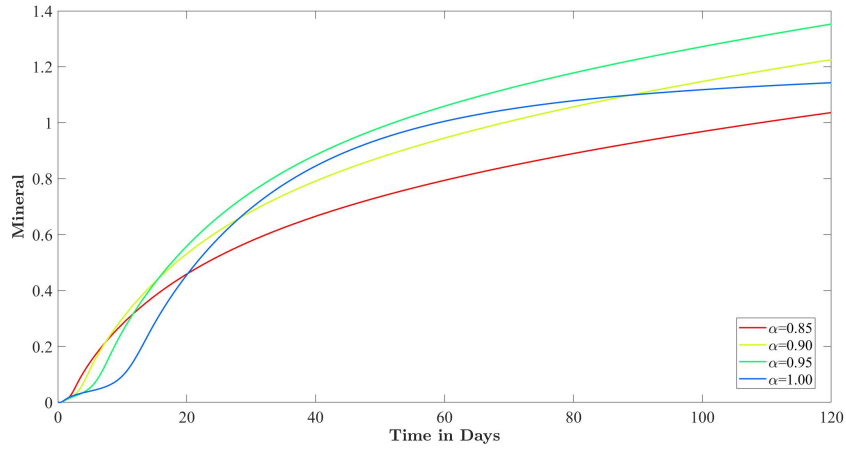


Figure 6: Variation in the quantity of the mineral with time for different value of $\alpha = 0.85, 0.90, 0.95, 1$.

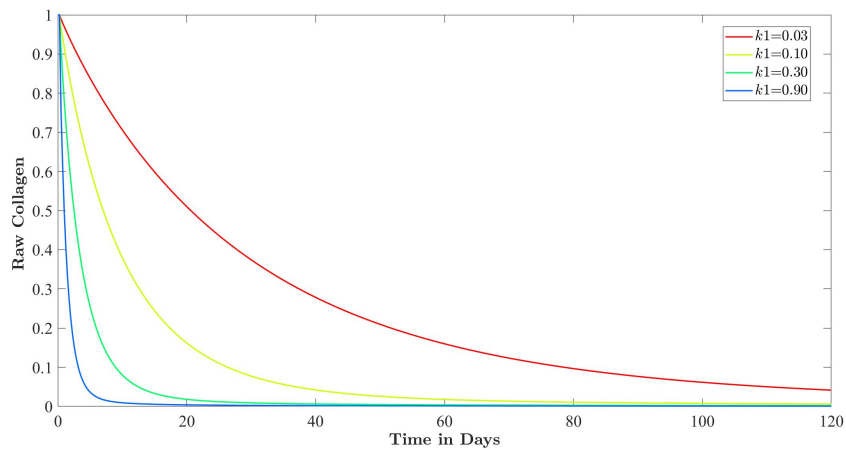


Figure 7: Impact of parameter k_1 (collagen cross-linking rate) on raw collagen for fractional order $\alpha = 0.95$.

5.1 Sensitivity Analysis

Parameters play a vital role in the dynamics of any system. Here, the impact of the various parameters k_1, k_2, v_1, r_1, r_2 has been studied on the model variables.

In figure 7, sensitivity with respect to parameter k_1 has been explored which concludes that as the rate k_1 increases (i.e. collagen cross-linking rate) raw collagen takes less number of days to transform into mature collagen. Here, precisely the effect is observed by increasing the rate to threefold.

Figure 8 provides a visual representation of how the parameter k_1 impacts the dynamic of mature collagen. So, we find that for different values of k_1 mature collagen reach equilibrium at a different level, and in general the number of mature collagen increases with time, and at a certain time, it reaches equilibrium, With the increase in the value of k_1 , the rate of formation of mature collagen increases. Figure 9 explores the impact of parameter v_1 on inhibitors. It highlights that as

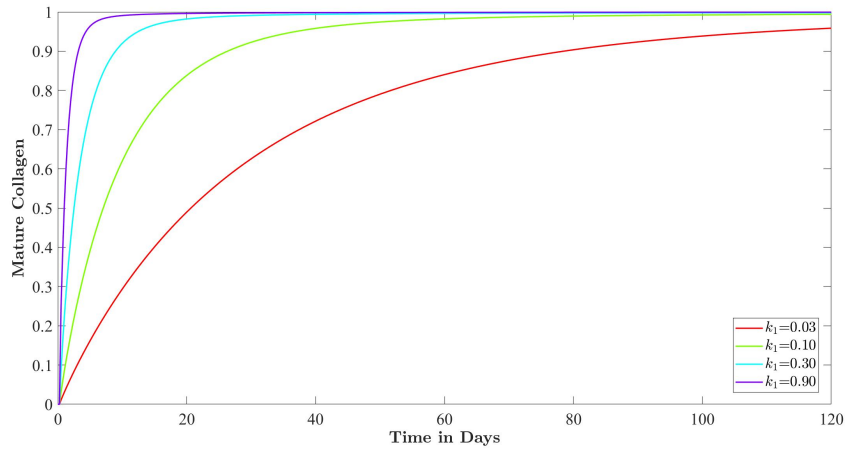


Figure 8: Impact of parameter k_1 (collagen cross-linking rate) on mature collagen for fractional order $\alpha = 0.95$.

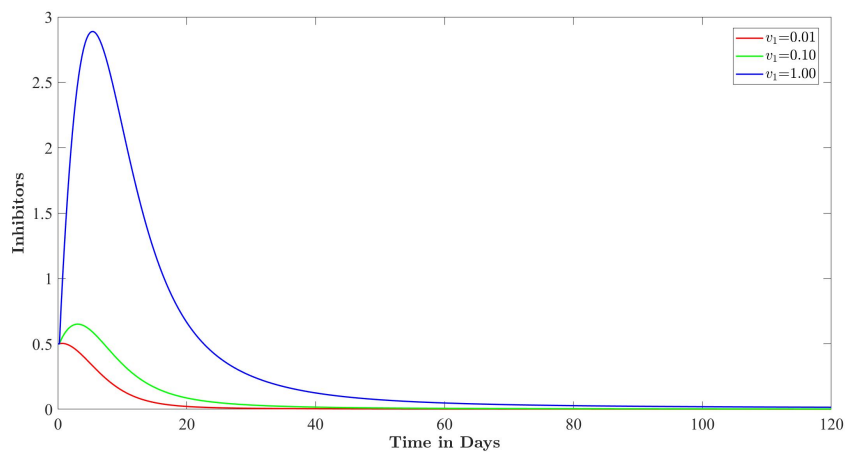


Figure 9: Impact of parameter v_1 (rate at which inhibitors diffuse) on inhibitor for fractional order $\alpha = 0.95$.

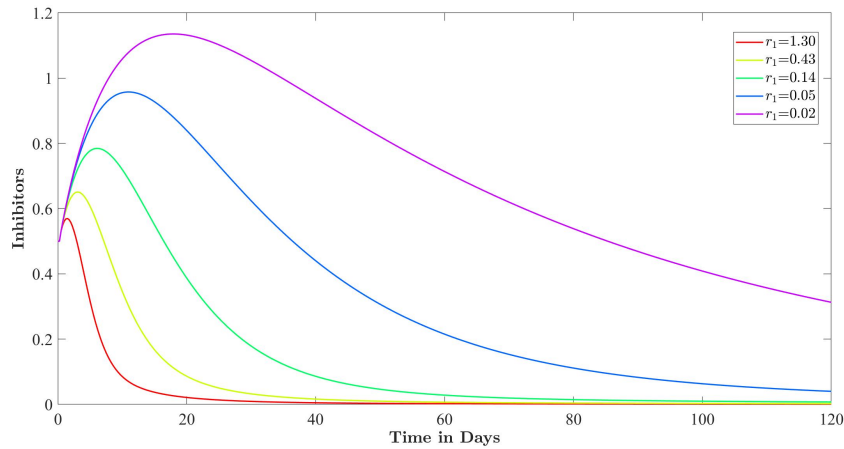


Figure 10: Impact of parameter r_1 (rate of inhibitor removal) on inhibitor for fractional order $\alpha = 0.95$.

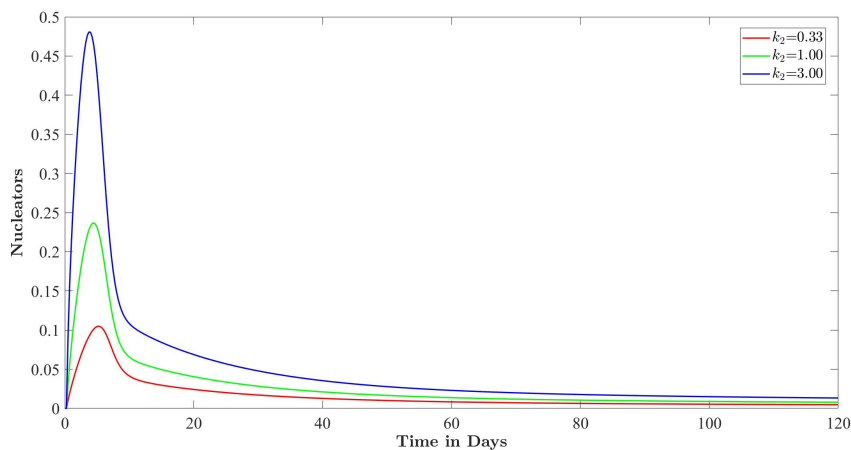


Figure 11: Impact of parameter k_2 on nucleators for fractional order $\alpha = 0.95$.

the parameter v_1 rises, more inhibitors will begin to diffuse into raw collagen. It is observable that there is a direct relationship between v_1 and inhibitor supply. There is a drastic increase in the concentration of active inhibitors for $v_1 = 1.0$. Figure 10 explores the impact of parameter r_1 on inhibitors. It depicts that the inhibitor’s concentration drops as the parameter r_1 increases because r_1 is the rate of removal of inhibitors and hence deterioration takes place largely.

Figure 11 explores the impact of parameter k_2 on nucleators. The nucleation process accelerates as the number of nucleators per mature collagen increases.

Figure 12 explores the impact of parameter r_2 on the nucleators. The number of nucleators grows as r_2 increases. As we increase the rate of r_2 three times we observe that the number of nucleators begins to diminish as they are masked by minerals.

Figure 13 explores the impact of parameter k_3 on mineralization. Mineralization is strongly linked to the parameter k_3 ; as the rate k_3 rises, so does mineralization. Changes in k_3 had a predictable effect on the pace of mineral production, but they also had a dramatic and proportionate effect on the degree of mineralization. A

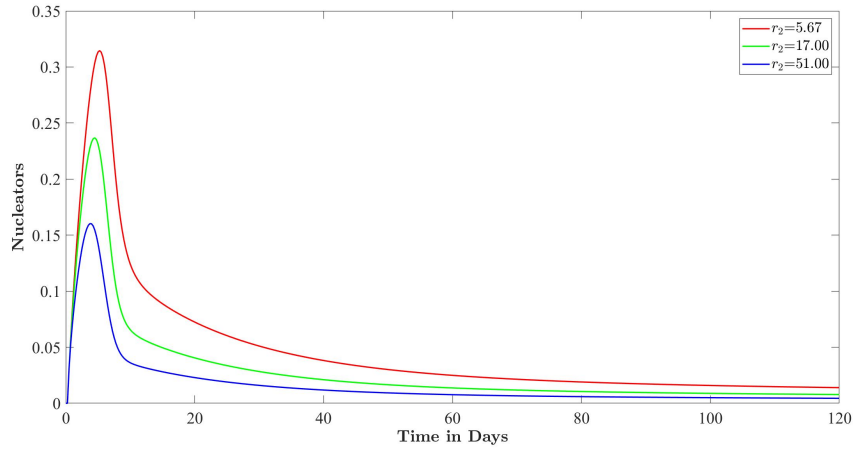


Figure 12: Impact of parameter r_2 on nucleators for fractional order $\alpha = 0.95$.

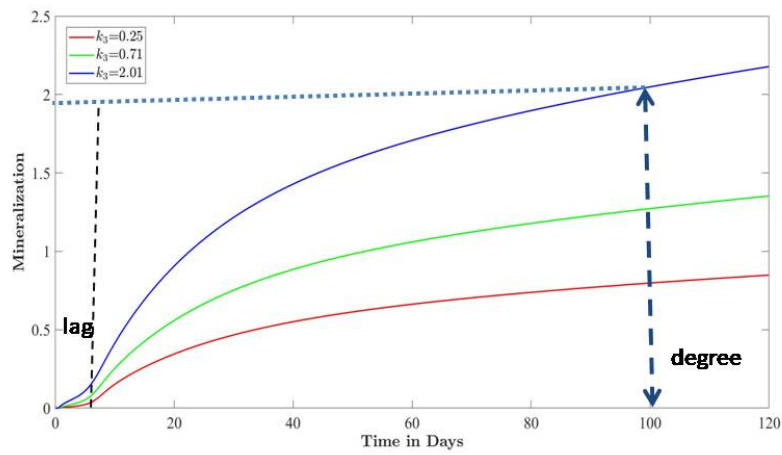


Figure 13: Impact of parameter k_3 on mineralization for fractional order $\alpha = 0.95$.

threefold drop in the rate of mineral formation k_3 resulted in a threefold decrease in mineralization degree.

The impact of all the parameters have been tested with raw collagen, mature collagen, inhibitors, nucleators, and mineralization but it is found that k_1 is the key parameter for raw and mature collagen whereas v_1 and r_1 are the key parameter for inhibitors k_2 and r_2 for nucleators and k_3 for mineralization respectively. Thus, it can be winded up with a graphical representation in the context of these parameters only. The CPU time taken for the computation in the code varies depending on the specific hardware and processing capabilities of the machine running the MATLAB code. The computation for the solution of this dynamical system took 1.9034 seconds of CPU time.

6 Conclusion

In this work, bone mineralization is studied with mathematical and numerical tools by considering bone at the micrometer level and thus provides vital support for the interpretation of experimental results. Furthermore, fixed point theory has been used to demonstrate the existence of a unique solution to the model. Also, the efficiency of the proposed scheme is drowned in terms of numerical simulations which are shown in graphs and it is clear that the proposed method is very accurate. Sensitivity analysis shows how the stiffness of bone depends on the inhibitor, nucleator, or raw or mature collagen and also to what extent bone does not get deformed under load. The use of fractional calculus helps in the early detection of any unusual patterns in the mineralization process. We can use this model to investigate more bone-related diseases by considering more assumptions. The obtained results will be useful for orthopedists to have a rough guess of the days needed for the mineralization of bone. Also, this model can be helpful for studying bone mineralization in other species too. A further important application is the study of how pharmaceutical therapies interfere with bone mineralization. The model can be modified to investigate the mineralization of additional calcified tissues, including the enamel, cementum, and dentin of teeth, etc.

Acknowledgement

The authors express their gratitude to the anonymous reviewers for their insightful recommendations aimed at raising the article's quality.

References

- [1] Agarwal, R., Airan, P., and Midha, C. (2023). Mathematical analysis of the dynamics of bone mineralization. In Singh, H., editor, *Mathematical Methods in Medical and Biological Sciences*. Elsevier, In press.
- [2] Agarwal, R., Purohit, S. D., and Kritika (2019). A mathematical fractional model with nonsingular kernel for thrombin receptor activation in calcium signalling. *Mathematical Methods in the Applied Sciences*, 42(18):7160–7171.

- [3] Atangana, A. and İğret Araz, S. (2021). 2 - two-steps lagrange polynomial interpolation: numerical scheme. In Atangana, A. and İğret Araz, S., editors, *New Numerical Scheme with Newton Polynomial*, pages 11–112. Academic Press.
- [4] Bozkurt, F., Yousef, A., Baleanu, D., and Alzabut, J. (2020). A mathematical model of the evolution and spread of pathogenic coronaviruses from natural host to human host. *Chaos, Solitons & Fractals*, 138:109931.
- [5] Caputo, M. (1967). Linear models of dissipation whose Q is almost frequency independent—II. *Geophysical Journal International*, 13(5):529–539.
- [6] Dey, P. (2020). Bone mineralisation. In Churchill, D. G., Sikirić, M. D., Čolović, B., and Milhofer, H. F., editors, *Contemporary Topics about Phosphorus in Biology and Materials*, chapter 3. IntechOpen, Rijeka.
- [7] Diethelm, K. and Ford, N. J. (2002). Analysis of fractional differential equations. *Journal of Mathematical Analysis and Applications*, 265(2):229–248.
- [8] Feng, Y.-Y., Yang, X.-J., and Liu, J.-G. (2020). On overall behavior of Maxwell mechanical model by the combined Caputo fractional derivative. *Chinese Journal of Physics*, 66:269–276.
- [9] Friedman, A. (2007). Mathematical analysis and challenges arising from models of tumor growth. *Mathematical Models and Methods in Applied Sciences*, 17:1751–1772.
- [10] Grodins, F. S., Buell, J., and Bart, A. J. (1967). Mathematical analysis and digital simulation of the respiratory control system. *Journal of Applied Physiology*, 22(2):260–276.
- [11] Komarova, S. V., Safranek, L., Gopalakrishnan, J., Ou, M.-j. Y., McKee, M. D., Murshed, M., Rauch, F., and Zuhr, E. (2015). Mathematical model for bone mineralization. *Frontiers in cell and developmental biology*, 3:51.
- [12] Kritika, Agarwal, R., and Purohit, S. D. (2021). A fractional model to study the diffusion of cytosolic calcium. In *Congress on Intelligent Systems: Proceedings of CIS 2020, Volume 2*, pages 585–597. Springer.
- [13] Sene, N. (2022). Analytical solutions of a class of fluids models with the Caputo fractional derivative. *Fractal and Fractional*, 6(1):35.
- [14] Shaikh, A. S., Shaikh, I. N., and Nisar, K. S. (2020). A mathematical model of COVID-19 using fractional derivative: outbreak in India with dynamics of transmission and control. *Advances in Difference Equations*, 2020(1):373.
- [15] Singh, H. (2020). Analysis for fractional dynamics of Ebola virus model. *Chaos, Solitons & Fractals*, 138:109992.
- [16] Singh, H. and Dutta, H. (2023). *Computational Methods for Biological Models*, volume 1109. Springer Nature.

- [17] Singh, J., Gupta, A. D., and Baleanu, D. (2023a). Fractional dynamics and analysis of coupled Schrödinger-kdv equation with Caputo-Katugampola type memory. *Journal of Computational and Nonlinear Dynamics*, 18(9):091001.
- [18] Singh, J., Gupta, A. D., and Kumar, D. (2023b). Computational analysis of the fractional Riccati differential equation with Prabhakar-type memory. *Mathematics*, 11(3):644.
- [19] Singh, R., Mishra, J., and Gupta, V. K. (2023c). The dynamical analysis of a tumor growth model under the effect of fractal fractional Caputo-Fabrizio derivative. *International Journal of Mathematics and Computer in Engineering*, 1(1):115–126.
- [20] ul Rehman, A., Singh, R., and Singh, J. (2022). Mathematical analysis of multi-compartmental malaria transmission model with reinfection. *Chaos, Solitons & Fractals*, 163:112527.
- [21] Veerasha, P., Prakasha, D., and Baskonus, H. M. (2019). New numerical surfaces to the mathematical model of cancer chemotherapy effect in Caputo fractional derivatives. *Chaos: An Interdisciplinary Journal of Nonlinear Science*, 29(1):013119.